

Investigating the effect of concentration of D-glucose on the optical rotation of white light.

R. Smith (C. Su, C. Sargent and S. Robinson)

L2 RLI, Class M, Team 3

Submitted: March 26, 2021

Optical rotation has an ever increasing importance in technology, in this work we measure the effects of optical rotation of white light through a solution of D-glucose of varying concentrations. Optical rotation has a wavelength dependence which in conjunction with Malus' Law forms a theoretical model of the resulting spectra. The observed spectra are collected with a 3D printed optics rail and USB web camera and we find that the data does not fit the theoretical prediction. The main reason for this is that the camera had auto exposure which made the small change in angle from optical rotation correspond to a small change in intensity which we could not distinguish from random error. We discuss the procedure of performing this experiment as well as improvements in the method for future investigation.

I. INTRODUCTION / THEORY

Introduction: The 19th century saw a large improvement in the understanding of the nature of light through the discovery of polarisation. The term polarisation was first coined by Étienne Louis Malus in 1808 whilst observing reflected light from a window pane through a calcite crystal [1] further investigations lead him to formulate Malus' Law. In 1815 Jean Baptiste Biot first observed optical activity through turpentine (a fluid obtained by the distillation of tree resin) [2]. This discovery allowed for a quantitative measure of concentration in sugar trading and formed the basis for chiral chemistry. Recent developments in this field has lead to applications such as liquid crystal displays and determining the absolute configuration of compounds using computational methods [3].

In this work we investigate the optical activity of D-glucose solution at various concentrations through analysis of white light spectra. We create and compare a theoretical spectra against the observations. Due to an oversight in the experimental design no strong conclusions can be gathered from the data. However we discuss the merits and flaws of the experimental design as well as improvements for future research.

Theory: Consider an unpolarised light source incident on a linear polarising filter (called the polariser). If the resulting polarised light is incident on another linear polarising filter (called the analyser) the change in intensity through the analyser is given by Malus' Law [1]:

$$I = I_0 \cos^2(\theta_i) \quad (1)$$

where I is the intensity after the analyser, I_0 the intensity before the analyser and θ_i the angle between axes of polarisation of the filters.

Glucose an optically active biological molecule has two optical forms the naturally occurring D-glucose and a synthetically produced L-glucose. These forms rotate the plane of plane polarised light in opposite directions. The amount of rotation is quantified by the specific rotation given by

$$[\alpha]_{\lambda}^T = \frac{\alpha}{l \times c} \quad (2)$$

where $[\alpha]_{\lambda}^T$ is the specific rotation at temperature T and wavelength λ , α is the measured rotation in degrees, l is the path length in decimeters and c is concentration in $\text{g}\cdot\text{ml}^{-1}$. For D-glucose this is given as $+52.7 \text{ deg}\cdot\text{mL}\cdot\text{g}^{-1}\cdot\text{dm}^{-1}$ [4] at room temperature with the wavelength being the Sodium D-Line (589 nm). The plus symbol indicates a clockwise rotation for an observer acting as the receiver. The relation

between specific rotation and wavelength is given by the Drude expression

$$[\alpha]_{\lambda}^T = \frac{A}{\lambda^2 - \lambda_0^2} \quad (3)$$

where A is $1.72 \cdot 10^7 \text{ deg}\cdot\text{ml}\cdot\text{nm}\cdot\text{g}^{-1}\cdot\text{dm}^{-1}$ and λ_0 is 150 nm at room temperature [5]. These values have a weak dependence on temperature however we assume these values are constant in the experiment.

II. METHODS

Apparatus: The main features of the apparatus are shown in Figure 1. The optics rail was constructed from 6 mm (diameter) wooden dowel and 3D printed PLA mounts. The models were made in SolidWorks and the printable parts are accessible in the **additional files**. The optics rail allowed for stable alignment and quick adjustments to obtain the clearest quality spectra. The lens had extrusions every 10° to align with a central mark on the lens holder for clear adjustments of angles. A 12 mm outer diameter quartz cuvette was used as incident light did not scatter or absorb a significant amount whilst traveling through the inner diameter (path length). Initial trials with cheap plastic cuvettes yielded poor results as the plastic itself caused optical rotation. The camera used was the KKEMOO USB 2.0 Web Camera. It had manual focusing so it could keep consistent focus between measurements. The diffraction grating had 600 lines per mm, this was the grating (out of the available) that gave the best quality spectra. The surroundings were kept dark by placing the apparatus inside a cardboard box. The external light source was shone through a pinhole in the cardboard and was aligned so that the beam went through

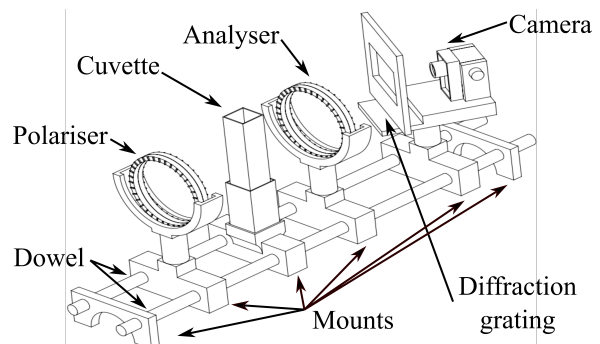


FIG. 1: Schematic of optics rail used to measure optical rotation through D-glucose

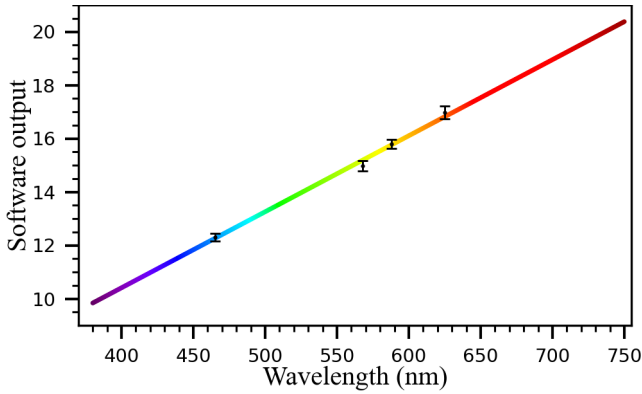


FIG. 2: The calibration curve using 4 LEDs of known wavelength

the filters, cuvette and diffraction grating. It was found that a pinhole produced the sharpest spectra. The camera and polarising filter were free to rotate and set to an angle such that the light from the pinhole was not in frame. This ensured that the software calculation of intensity worked as intended. There were multiple spectra visible in the frame however only the data from the brightest spectra was taken as that minimised the significance of random noise. The cardboard box and the apparatus were painted black to reduce the effect of scattering from the cuvette. The light source, box and apparatus were held into place with black electrical tape to prevent movement whilst the cuvette or angle was changed.

Method for taking results and analysis: The software used to gather spectra data was Theremino. For each required spectra 30 readings were taken in Theremino and averaged in Python. This was to reduce the effect of random noise from the individual samples. Theremino only measures relative intensity. To allow for comparison between spectra of different angles the data is normalised by subtracting the lowest value (background noise) of each spectra to the whole of the spectra.

Calibration can be done in Theremino, however to include more calibration points and increase reliability Python was used. Calibration was performed by comparing the (Theremino) wavelength of the peak intensity of LEDs to the known wavelength. During calibration the polarising filters and cuvette were in place so the calibration conditions were the same as experimental conditions. The axes of

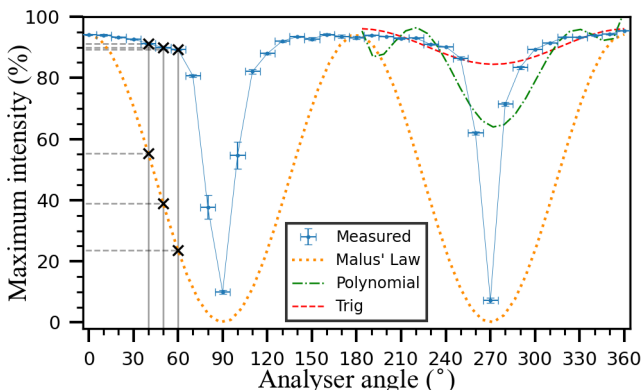


FIG. 3: Measured intensity for varying analyser angle with different models

polarisation were set 0° degrees to reduce the significance of noise. This position is found by finding the minimum (which is an easier spectrum to observe) then rotating by 90° . The averaged spectra are used to generate a calibration curve fitting the known wavelength of the LEDs. A linear model can be fit using chi-squared minimisation with the weighting given by the full width half maximum (FWHM) of the peak. This means that LEDs with a narrower peak are considered more important thus making the conversion more reliable.

Peak intensity can be plotted against analyzer angle to show how intensity changes with angle. Different models can be fit to the curve with the best fit acting as a theoretical model for how small changes in angle affect the intensity of the light. Considering Eq.(3) predictions can be made to how much the specific rotation should change for different wavelengths. This is used to predict intensities for the change of concentrations in the solution.

Glucose was used as the optically active medium as it was easy to obtain. The values of concentration were chosen to be less than the saturation of the solution to avoid additional absorption. The water was left out for 30 minutes to reach room temperature and data was taken when the analyser angle was 30° , 40° and 50° . These angles were predicted to give the highest change in intensity for a small change in angle.

III. RESULTS

The calibration curve using blue (465 nm), green (568 nm), yellow (588 nm) and red (625 nm) LEDs is shown in Figure 2 with the wavelength ranging from 380 nm to 750 nm which is around the range of visible light [6], the dependent variable is along the x-axis for clarity. The Goodness of fit statistics for this line are shown in Table 1 which show a reasonable fit. The maximum intensity of the spectra against angle of the analyser is shown in Figure 3 alongside Malus' Law and two additional models that are fitted to the data. The Trig model was fit to the whole range of angles and the polynomial from $0-180^\circ$ however they are transformed to lie on the $180-360^\circ$ range for clarity. There is visible deviation from Malus' Law in the experimental data. The results of the chi-squared analysis for the different models are shown in Tab. 1 showing that the models do not fit the data. The averaged spectra for different concentrations (at 50°) are plotted in Figure 4 (A) with $0.00 \text{ g}\cdot\text{ml}^{-1}$ highlighted with blue dashes and $0.40 \text{ g}\cdot\text{ml}^{-1}$ highlighted with black dash-dots. The error in the wavelength for this and other graphs is not plotted for clarity. The difference between intensity of the averaged concentrations is shown in Figure 4 (B) alongside the theoretical prediction (which is approximately 0), the error bars from the theoretical model form a tolerance for the difference between observation and theory and are shown by the thin solid black

Curve/Model	DoF	χ^2_{min}	χ^2_ν	$P(\chi^2_{min};\nu)$
Calibration	2	1.917	0.959	0.383
Malus' Law	37	62492910	168900	0.000
Polynomial	11	979332	89030	0.000
Trig	34	30570	900	0.000
Δ conc	129	449	3.480	5.607 (e-37)

TABLE I: Goodness of fit statistics for plots

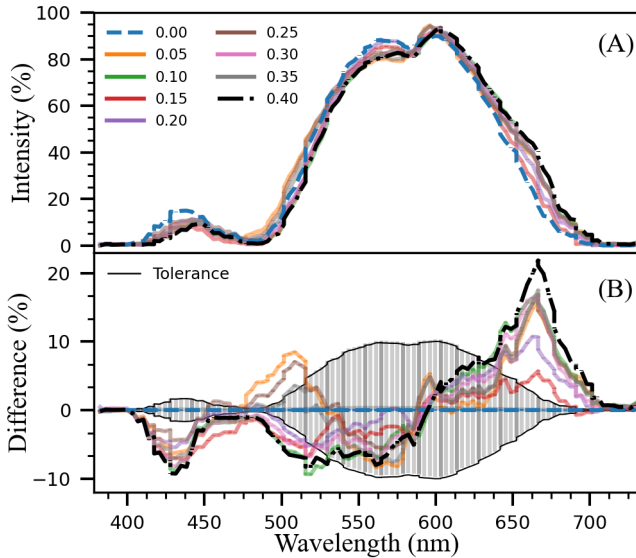


FIG. 4: (A) Spectra for different concentrations of D-glucose. (B) The difference between concentration spectra and water.

line. We can see that the observed difference does not match the theoretical prediction from the chi-squared values given in Tab.1.

IV. DISCUSSION

We expect the relation between the software wavelength and true wavelength to be a linear model which we observe in Fig. 2. The line extends to cover the range of wavelengths of the white light spectrum. The linear model fits the data well as seen from Tab.1. We take the null hypothesis that the discrepancies between prediction and observation can be explained by random error. We have that the $\chi_{min}^2 \approx \text{DoF}$ (Degrees of Freedom, " ν "), that $\chi_{\nu}^2 \approx 1$ which is within $\pm 2\sigma$ of the DoF ($\nu - 2\sqrt{2\nu} \leq \chi_{min}^2 \leq \nu + 2\sqrt{2\nu}$ and $P(\chi_{min}^2; \nu) \approx 0.5$ which implies that we reject the null hypotheses at the 5% level. At 0° we set the intensity of the Malus' Law plot to that of the measured value to allow us to compare the theory to observed results. The observed intensity does not match what we expect for Malus' Law shown in Fig. 3. The angles of maximum and minimum intensity are periodic which is what we expect however there is significant deviation between these maximum and minimum angles.

Quantitatively we can see that Malus' Law does not fit from Tab. 1. The χ_{min}^2 and χ_{ν}^2 are both very large and $P(\chi_{min}^2; \nu) \approx 0$, hence we can reject the null hypothesis. The trigonometric (Trig) function given by

$$\alpha \cdot \cos^2(\theta - \beta) + \gamma \quad (4)$$

was fit to the data where α, β and γ are parameter values and θ is the analyser angle. A polynomial of degree 8 given by

$$\sum_{i=0}^8 c_i \cdot \theta^i \quad (5)$$

was also fit to the data where c_i are the parameter values. A degree 8 polynomial was chosen as it gave the lowest

χ_{min}^2 value for polynomials of degree 0-8 and the numerical method used to optimise the parameter values did not converge at a degree 9 polynomial or higher.

The degrees of freedom of the models match what we expect considering the number of parameters and the range across which the models are fit. The polynomial is fit to only half the angle range to reduce the problems of numerical convergence. Similarly to the Malus' Law fit the other model have very large χ_{min}^2 and χ_{ν}^2 and $P(\chi_{min}^2; \nu) \approx 0$. Hence we reject the null hypothesis for all of the models at 5% level. The Polynomial fit is worse than the Trig as it over and undershoots the data points with the smallest uncertainty. The fit models struggle to accurately map the dip in intensity. These points have the highest uncertainty due to the greater significance of noise at lower intensities, hence have smaller chi-squared weightings. As no model has a good fit we used an empirical model to make predictions. We used a linear model between data points (fitted with chi-squared weightings) to produce a function that takes an angle (not directly measured) and gives back its predicted intensity with associated error.

When planning the experiment, we assumed that the observed intensity would follow Malus' law. This allowed us to predict which angles gave the greatest change in intensity for a small change in angle. Thus the small change in angle due to optical rotation would obtain a large change in intensity. These angles are marked by the solid black line in Fig. 3. We can see that the intersections with the Malus' Law plot lie on the steepest gradient of the plot however this is not true of the measured plot. At these angles the measured plot has a much shallower gradient hence a small change in angle causes a small change in intensity. This is a large problem as we predict that the observed changes will be very small and random error will have more significance.

Why does Malus' Law not hold in this case? The reason for the large deviation between Malus' Law and the experimental data is the auto exposure feature of the webcam. For example, consider the $0-90^\circ$ range, as the angle increases from 0° the maximum intensity of the spectra should go down as less light can pass through the anal-

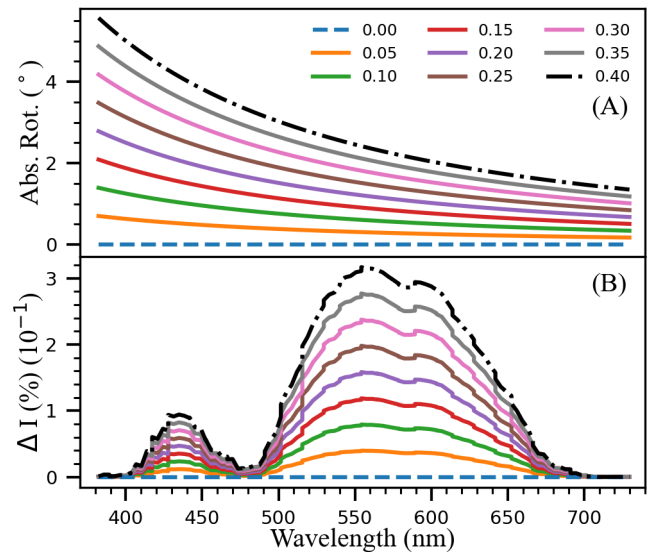


FIG. 5: (A) Absolute rotation of white light through the cuvette (B) Predicted difference in intensity for different concentrations

user filter. However as brightness decreases the aperture of the camera increases causing the sensor in the camera to be more exposed, hence the apparent intensity of the spectra remains large. We observe a small decrease in intensity in the 0-60° range as the additional aperture size causes an increase in background intensity hence during normalisation the resulting intensity would have decreased. We suggest that at around 60° the maximum aperture of the camera is reached and beyond this point we expect a decreasing intensity as angle increases up to 90°. At 90° it matches Malus' Law as the minimum. Subtracting the lowest intensity from each spectrum accounts for background noise however there is still an offset from zero observed at the minimum of the plot. A possible explanation is that some of the light is scattered by the solution and reflected off the polarising filter as it has a slightly glossy finish. This increases surrounding brightness (despite the equipment being painted black).

We observe small differences of spectra between the concentrations in Fig. 4A. Measuring the path length of the cuvette we predict using Eq.(2) the absolute rotation for each concentration shown in Fig. 5A. We observe that higher concentrations produce more rotation and that shorter wavelengths are rotated more. At the concentrations of D-glucose obtained the predicted rotation would be small hence the predicted change in intensity will be small.

We used the maximum difference in optical rotation to test against measurement. This was the difference between 0.40 g·mL⁻¹ and 0.00 g·mL⁻¹. The theoretical difference without uncertainty is given in Fig. 5B, the plot with errors shown is the tolerance curve in Fig. 4B. Excluding the errors we observe an increasing difference in intensity as concentration increases however this is not what we observe in Fig. 4B. It appears that the 0.40 g·mL⁻¹ has the maximum difference but we obtain negative values and observe large variations not seen in the prediction. Chi-squared analysis against the prediction is performed on the difference in intensity of the 0.40 g·mL⁻¹ curve shown in Tab. 1. The χ_{min}^2 and χ_{ν}^2 are both large and $P(\chi_{min}^2; \nu) \approx 0$, hence we can reject the null hypothesis.

Most of the curve between 530 and 640 nm lies within the tolerance curve however there are large deviations at 430 and 670 nm. This can be explained by considering Fig. 2. The points of maximum deviation occur outside the range of the calibration points hence we are extrapolating the calibration curve and in doing so we lose reliability in the conversion. The small predicted difference means that the data collected is sensitive to the conditions of the setup and small changes in the experimental apparatus from opening and closing the box, rotating the polarising filter and changing the cuvette will significantly affect the result.

How was the method? Many precautions were taken to reduce the errors in the experiment, the equipment was painted black which made a noticeable difference in reducing background light. The optics rail successfully managed to keep everything aligned and consistent between readings however the box itself was susceptible to movement allowing for small variations in alignment between measurements. The largest problem in the method was the camera having auto exposure this caused the difference in intensity to be very small hence increasing significance of random errors. The amount of rotation in the concentration of glucose was small however this might not have been a problem if the camera did not have auto exposure.

Have all the errors been taken into account? There were small affects that were not taken into account like the nudges to the box after each measurement and the lean of the polarisation filters sitting in the mounts, this would have changed the incident polarisation slightly (Malus' Law requires both polarising filters to be parallel) however this was not a major source of error in the experiment.

How could the method be improved? Clearly the main thing to improve this experiment would be the camera, if it did not have auto exposure, we would have got a better fit with Malus' law hence we would have managed to get a detectable difference in intensity for the optical rotation. Absolute intensity could have been calculated using a charge-coupled device (CCD) which would allow more reliable comparison between angles. Sucrose could have been used as the optically active medium as it has a slightly higher specific rotation compared to glucose at +66.37 deg·mL·g⁻¹·dm⁻¹ [4]. To increase the absolute rotation we could have increased the size of the cuvette, although scattering and absorbance would need to be accounted for. Using a diffraction grating with higher lines per mm could have improved sharpness of the spectra.

During calibration a wider range of LED wavelengths would have made the calibration more accurate. Using a tuneable laser would allow a highly accurate calibration curve however these are costly. A white light optical fibre could be used to produce a high intensity source with small beam width hence allowing a larger path length, more rotation and a greater change in intensity.

V. CONCLUSIONS

Our main objective was to measure the effect of concentration of D-glucose on the rotation of white light. Using a homemade optics rails and performing data analysis to form a predicted model we could draw no strong conclusions from the data. Our results deviated from Malus' Law and did not match the theoretical predictions. This was due to the camera having an auto exposure feature meaning that the change in intensity from the optical rotation was too small and susceptible to random error. The 3D model files and potential improvements were given to aid in future research.

VI. ADDITIONAL FILES

https://github.com/RobSmith2000/RLI_Prints

References

- [1] É.L Malus, '*Mémoires de Physique et de Chimie de la Société d'Arcueil, (2nd ed.)*', la Société d'Arcueil, Paris (1809)
- [2] J.B Biot, '*Bulletin des sciences Société*', Philomathique de Paris, Paris:Plassan (1815).
- [3] P. J. Stephens et al., '*Determination of Absolute Configuration Using Optical Rotation Calculated Using Density Functional Theory*', ACS Publications (2016), accessed 24 March 2021 <https://doi.org/10.1021/oi0201714>
- [4] R. C. Weast, '*Handbook of Chemistry and Physics (55th ed.)*', CRC Press(1974)
- [5] C. Stark et al, '*Broadband polarimetric glucose determination in protein containing media using characteristic optical rotatory dispersion*', Biomed. Opt. Express 10 (2019)
- [6] C. Starr, '*Biology: Concepts and Applications*', Thomson Brooks, Belmont CA (2005)

VII. ERROR APPENDIX

Individual Measurements: The error in angle and path length is given by half the smallest division of the measuring device ($\pm 5^\circ$ and ± 0.5 mm respectively). The volume of water and mass of glucose were measured using a top pan balance accurate to 0.01 g hence error in the concentration was found by using calculus-based approximations [This and all other equations in this section are from I. G. Hughes and T. P. A. Hase, *Measurements and their Uncertainties*, Oxford University Press, Oxford (2010)]

$$Z = \frac{A}{B} \implies \frac{\alpha_Z}{Z} = \sqrt{\left(\frac{\alpha_A}{A}\right)^2 + \left(\frac{\alpha_B}{B}\right)^2} \quad (6)$$

where A , B and Z are variables and α_A , α_B and α_Z are the associated errors. The average error across the range of concentrations was found to be $\pm 5 \times 10^{-4}$ g·mL $^{-1}$. The error in the Thermano output was taken as half the resolution of the intensity and wavelength given as ± 0.05 % and ± 0.05 units (± 1.3 nm) respectively. These are small compared to the other errors, so we assume they are negligible whilst propagating through the functions.

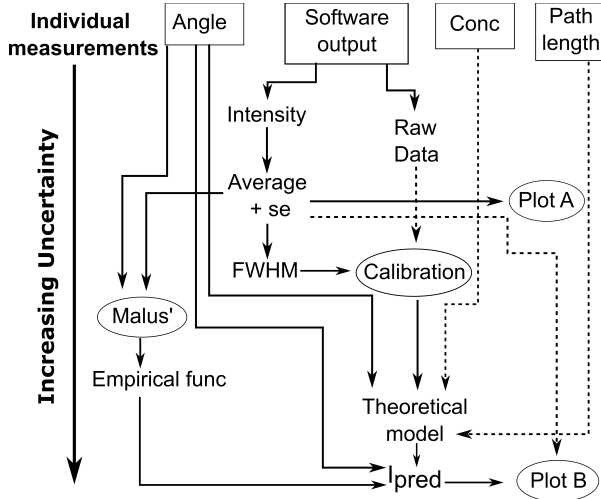


FIG. 6: Flow diagram showing dependencies of errors functions used in producing plots

Propagation of errors: We propagate the errors from the individual measurements through functions using the functional approach. The dependency of functions to other errors is given in Figure 6 where Plot A is Fig. 4A and Plot B is Fig. 4B. The individual measurements are highlighted in boxes and the resulting graphs are highlighted in ellipses. The overall error in each function increases as we descend Fig. 6. The solid arrows represent significant contributions to the error whereas dotted arrows represent contributions that are negligible.

The average intensity and standard error for a given concentration and rotation is found by taking the average and standard error of each data point in the spectra for 30 spectra. The Empirical function is fit to a linear model using chi-squared minimisation. For all the chi-squared minimisations we use the Broyden–Fletcher–Goldfarb–Shanno (BFGS) algorithm as we are trying to solve a nonlinear unconstrained optimisation. In the empirical model and calibration curve we calculate errors using the inverse Hessian which is numerically approximated at each step from the BFGS algorithm. The error in the parameters is given by

$$\sigma_i = \sqrt{2 \cdot \mathbf{H}_{ii}^{-1}} \quad (7)$$

where σ_i is the standard deviation of the i th parameter and \mathbf{H} is the Hessian.

The optimised values in parameter space for the calibration curve are shown in Figure 7 with elliptical contours at 1, 2 and 3 standard deviations away from the optimum value. The optimum values obtained for the intercept and gradient are -0.9 ± 0.8 and 0.0285 ± 0.0014 nm $^{-1}$ respectively which is verified by the scale of the axes in Fig. 7.

The errors in concentration and path length are small compared to the other errors so are neglected in the theoretical model. The standard error of the average of the curves are neglected in plot B as the induced errors from propagation in the predicted intensity are much larger.

The uncertainty in the parameters values as well as the errors in angle are the dominant errors in the theoretical model and predicted intensity which give rise to the dominant errors observed in the Plot B.

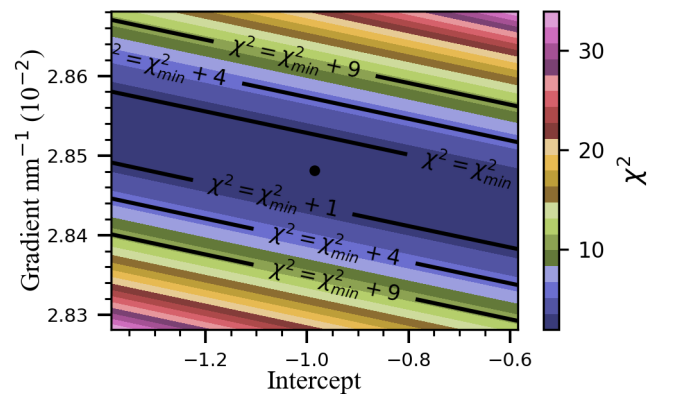


FIG. 7: Heat map and contour plot for optimum parameter values of the calibration curve